AGU PUBLICATIONS

JGR

Journal of Geophysical Research: Atmospheres

RESEARCH ARTICLE
10.1002/2017JD027861

Key Point:
- Including the contrails' ice water content dependence on temperature in off-line estimates reduces their radiative forcing uncertainties

Correspondence to:
R. Rodríguez De León,
r.deleon@mmu.ac.uk

Citation:
Rodríguez De León, R., Lim, L. L., Lee, D. S., Bennett, M., & Krämer, M. (2018). Simple versus complex physical representation of the radiative forcing from linear contrails: A sensitivity analysis. *Journal of Geophysical Research: Atmospheres*, *123*, 2831–2840. https://doi.org/10.1002/2017JD027861

Received 18 OCT 2017
Accepted 12 FEB 2018
Accepted article online 16 FEB 2018
Published online 9 MAR 2018

Simple Versus Complex Physical Representation of the Radiative Forcing From Linear Contrails: A Sensitivity Analysis

Rubén Rodríguez De León[1], Ling L. Lim[1], David S Lee[1], Michael Bennett[1], and Martina Krämer[2]

[1]Faculty of Science and Engineering, Manchester Metropolitan University, Manchester, UK, [2]Forschungszentrum, Jülich Institut für Energie und Klimaforschung Stratosphäre, Jülich, Germany

Abstract An off-line complex representation of the radiative forcing of linear contrails is applied for the first time to monthly mean 3-D distributions. This representation assumes the same temperature-dependent, spatially and time-varying functions of ice water content and particle size for contrails as for natural cirrus. This complex representation is contrasted with more commonly used simplified setups in which fixed contrail optical depth values [0.1 to 0.3] are prescribed and from which the results show differences covering a factor of 3 assuming fixed or variable contrail layer altitudes. This prescribed range of representative fixed altitudes resulted in differences covering a factor of 2 when the optical depth was also fixed. Prescribing fixed particle sizes also resulted in differences covering a factor of 2 if altitude and optical depth are also fixed. In contrast, the inclusion of the dependence of the contrail ice water content on temperature produced differences of around 20% or less when assuming the same ranges of altitudes and ice particle sizes, resulting in a much improved confidence in the radiative forcing estimates and more accurate spatial and temporal representations of the radiative interaction between contrails and the background meteorology. Assuming a contrail vertical extent of 500 m, a 9 mW m^{-2} annual mean contrail radiative forcing is estimated, with an uncertainty range between 1 and 23 mW m^{-2} based on the ice water content's observed variability.

1. Introduction

Linear contrails are estimated to contribute 10 mW m^{-2} (Boucher et al., 2013) to the radiative forcing (RF) from aviation, with an uncertainty range [5 to 30 mW m^{-2}] affected not only by the difficulties involved in the retrieval of their spatial distribution and their physical and radiative properties but also by the computational expense of fully representing these properties in large-scale models. It has for these reasons been common for off-line contrail studies to assume simplified representations of their physical and radiative properties; among them is the use of fixed values to prescribe their optical depth, ice crystal particle size, altitude, and vertical physical thickness. Most off-line contrail studies have assumed a fixed optical depth (e.g., Markowicz & Witek, 2011; Minnis et al., 1999; Myhre & Stordal, 2001; Rädel & Shine, 2008; Rap et al., 2010; Stuber & Forster, 2008; Yi et al., 2012), with values ranging between 0.1 and 0.3. In these studies a linear dependence of the contrail RF on their optical depth is assumed and it is therefore expected that observed optical depth time-averaged values will emulate the RF of the varying optical depth. Fixed contrail altitudes have also been commonly prescribed (e.g., De León et al., 2012; Markowicz & Witek, 2011; Minnis et al., 1999; Myhre & Stordal, 2001; Yi et al., 2012), and with the exception of De León et al. (2012, DL12 hereafter) all of these studies also prescribed fixed particle sizes.

The aim of the present work is to assess the RF uncertainties associated to such simplifications, by contrasting their results with those based on temperature-dependent ice water content (IWC) and ice particle size parameterizations applied off-line for the first time to a 3-D linear contrail cover distribution. This approach was previously applied by DL12, but it was limited to only two representative months, a 2-D contrail cover at fixed altitudes, and average day/night conditions. Here we extend these spatial and temporal representations by including the vertical distribution of linear contrails and the diurnal and monthly variation of traffic, allowing the reference case to incorporate a realistic dependence of the radiative properties of contrails on altitude, which was not possible in the DL12 setup.

Contrail cover fields can be calculated within a climate model (online) or be based on a prescribed background meteorology (off-line). The results of these two approaches tend to differ in the spatial and temporal correlation of contrail and natural cloud formation, as shown by Rap et al. (2010), and therefore in their vertical overlap. While online calculations are considered more realistic, climate models also present limitations in their meteorology and in the radiative representation of ice clouds (Waliser et al., 2009). For these reasons we also include in the present study sensitivity simulations for diurnal traffic variation and assumed overlap, in order to assess their associated uncertainties from a purely radiative perspective.

2. Model Setup

The model setup is similar to the one described in DL12, in which persistent contrails and natural cirrus were assumed to have the same IWC and particle size dependence on ambient temperature. This approach was applied in an early study by Ponater et al. (1996) and has more recently been supported by measurements such as those from the midlatitude field campaign CIRRUS III (Schäuble et al., 2009) showing that the IWC in cirrus and aged contrails is similar under the same atmospheric conditions, as well as from Krämer et al. (2016), who found slightly higher contrail IWCs at 210 K. The assumption is also supported by observations by Chauvigné et al. (2017), who reported that the optical properties, including extinction coefficients and phase functions, of old contrails and natural cirrus resemble each other. They also observed similarities in the particle size distributions (PSDs) of natural cirrus and contrails aged 290 s or less. The focus of the present study does not include the theoretical basis of contrail IWC evolution, but a description of the development of IWC measurements with respect to temperature can be found in Krämer et al. (2016).

2.1. Contrail Radiative Parameterizations

A radiative parameterization in terms of the contrails' IWC and particle size was derived by integrating the long-wave (LW) and short-wave (SW) single scattering properties of randomly oriented hexagonal prisms, developed by Baran et al. (2001) and Yang et al. (2000), respectively, over a set of bimodal PSDs taken from a parameterization developed by McFarquhar and Heymsfield (1997). In order to confirm that the PSDs were not affected by ice shattering contamination, DL12 showed that the total number of ice crystals from this parameterization matched quality-checked number concentrations reported in Krämer et al. (2009) at a representative range of latitudes. The PSD parameterization covered a representative range of temperature and IWC values taken from the climatology compiled by Schiller et al. (2008). These same PSDs were used in the simulations to prescribe the contrails' IWC and particle size, represented in the model by the generalized diameter (D_{ge}) defined in Fu (1996) as

$$D_{ge} = \frac{\int_{L\min}^{L\max} DDLN(L)\,\mathrm{d}L}{\int_{L\min}^{L\max} \left(DL + \frac{\sqrt{3}D^2}{4}\right) N(L)\,\mathrm{d}L}, \tag{1}$$

in which $N(L)$ denotes the number density per unit volume, $L_{\min}$ and $L_{\max}$ define the range of the maximum dimension of the particles present in the distribution, and D is the length of the diagonal of the hexagonal face.

The radiative databases currently available for single ice crystal shapes tend to incorporate size-dependent aspect ratios (D/L) only in the cases of pristine habits. It is for this reason that the volumes and projected areas of hexagonal prisms produced a better match to McFarquhar and Heymsfield (1997) measurements in the small and the large modes of their PSD retrievals, when compared to more complex shapes, for which fixed aspect ratios are normally assumed. For this reason hexagonal cylinders were the only habit considered in the simulations. This match ensured that the representation of the physical and radiative properties was physically consistent both in the parameterizations and in the prescribed IWC and D_{ge} combinations (De León & Haigh, 2007). These aspects are normally neglected when fixed optical depth or ice particle size values are prescribed.

The instantaneous RF, defined as the difference at the top of the atmosphere of the radiative fluxes with and without contrails, was calculated using the Edwards-Slingo two-stream radiative transfer code (Edwards & Slingo, 1996). Solar zenith angles and day lengths at the middle of the month were used to represent the monthly mean SW fluxes with a five-point Gaussian integration. The background meteorology for the radiative calculations used monthly mean values for temperature, water vapor, ozone, and surface albedo, from European Centre for Medium-Range Weather Forecasts ERA40 reanalysis data (Simmons & Gibson, 2000) and monthly mean cloud fields from the International Satellite Cloud Climatology Project D2 data set. Liquid water clouds consisted of spherical droplets with an effective radius of 10 μm, and all cloud layers were assumed to randomly overlap.

2.2. Contrail Cover

The contrail cover distribution was generated using the Contrail Modeling and Analysis tool (Lim et al., 2006), which is based on the contrail parameterization and the off-line methodology described in Appendix A of Sausen et al. (1998). The aircraft movements were based on the aircraft emissions data set used in the European research project REACT4C (Reducing Emissions from Aviation by Changing Trajectories for the benefit of Climate). The aircraft movements from the REACT4C base case (Søvde et al., 2014) were incorporated into the Future civil Aviation Scenario software Tool (FAST) emissions model to calculate the distance traveled for the year 2006. The global distance traveled, from ground level up to 44,000 ft (13.5 km) on 2,000 ft (600 m) intervals, was approximately 38.9 billion kilometers, with 87% occurring above 500 hPa. The diurnal distance traveled over four time bands (00, 06, 12, and 18 UTC) was coupled with European Centre for Medium-Range Weather Forecasts ERA-Interim meteorological data sets (regular grid, 2.5° × 2.5°) for the same year. The cloud cover from ERA-Interim was used by Contrail Modeling and Analysis tool to calculate the critical relative humidity for cloud formation (Lim et al., 2015). The specific humidity and temperature were then used to determine the potential and actual contrail coverage, assuming an aircraft fleet propulsion efficiency of 0.36 that resulted in an annual global contrail cover of 0.10%.

3. Simulations

The contrails' IWC parameterization was defined as a function of local ambient temperature, based on the mean IWC fit for nonconvective conditions from the IWC climatology compiled by Schiller et al. (2008). These combinations of IWCs and temperatures were incorporated into the PSD parameterization of McFarquhar and Heymsfield (1997) to prescribe the contrail's D_{ge}, resulting in a range between 14 and 41 μm when applied to the contrail cover, and IWCs between 0.015 and 10 mg/m^3 (3.7 mg/m^3 at 222 K).

Given the restriction in their radiative transfer model to single IWC and particle size values in each cell, in their sensitivity simulations DL12 emulated the contrails' IWC by rescaling the contrail layer's horizontal extent in cells that already contained natural cirrus, but this approximation tended to amplify the contrail RF dependence on the IWC's variation. For this reason in the present study the sensitivity simulations were performed under clear-sky conditions. A first set of simulations included natural clouds (all skies) and kept the model's original vertical layer resolution, which at relevant contrail altitudes was approximately 1,500 m. In the second set of simulations the contrails' IWC was modified in order to emulate a more realistic contrail thickness of approximately 750 m or to prescribe fixed contrail optical depth values. These simulations were performed under clear-sky conditions.

3.1. Sensitivity to Macrophysical Parameters

The simulations to assess the sensitivity to the assumptions on macrophysical aspects are described in Table 1, including the calculated annual mean RFs for each case and their percentage differences (shown in parentheses) with respect to the reference case. The corresponding monthly mean differences from Table 1 are presented in Figure 1.

The annual traffic case (reference case), which excluded the monthly variation of traffic, produced a net (SW + LW) RF of 24.9 mW m^{-2}, which is likely an overestimate linked to the 1,500 m contrail vertical thickness assumed in this set of simulations. The monthly traffic case, which incorporated not only the diurnal but also the monthly variability of traffic, showed negligible change in the annual mean net RF compared to the reference case and monthly mean differences within 10% (see Figure 1). In contrast, the no-diurnal case, in which the diurnal variation of traffic was neglected, produced a 21% net RF increment, caused by the increased nighttime traffic contribution from 38% to 50%. As a consequence of this increment, the corresponding nighttime contrail cover and net RF contribution changed from 35% to 47% and from 84% to 86%, respectively. Despite the limitations in the off-line contrail coverage approach, mentioned in section 1, a similar nighttime contrail net RF contribution (92%) to the one found here was reported by Chen and Gettelman (2013), based on online simulations in which a linear contrail lifetime of 30 min was assumed. In contrast, a previous off-line study by Stuber and Forster (2008) found a contribution of 60% despite reporting a similar net RF increment (20%) to the one found here, while Frömming et al. (2011) reported a net RF increment of only 6%.

The clear-sky case resulted in a 7% net RF reduction on the global mean despite some areas with low surface albedos showing enhanced net RFs. Previous contrail studies have reported enhanced RFs in their clear-sky simulations, but reductions can be expected from contrails with sufficiently large optical depths, as shown by Markowicz and Witek (2011) for fixed $\tau > 0.3$ (see their Figure 7).

Table 1
Description of the Contrail and Natural Cloud Cover Sensitivity Cases and Their Global Annual Mean RFs

Case	Description
Annual traffic (Ref)	Reference case. Complex representation (IWC and D_{ge} are functions of temperature with variable altitude) under all skies with random cloud overlap, and diurnal but no monthly variation of traffic. The vertical thickness at representative contrail altitudes is approximately 1,500 m.
Monthly traffic (monthly cover)	Same as Ref but including monthly variation of traffic.
Daily mean traffic (no diurnal)	Same as Ref but excluding diurnal variation of traffic.
Clear sky (clear sky)	Same as Ref but excluding natural clouds.
Maximum overlap (max overlap)	Same as Ref but assuming maximum random cloud overlap.

	Radiative forcing (mW m^{-2})					
	NET		LW		SW	
Annual traffic (Ref)	24.9		55.2		−30.3	
Monthly traffic (monthly cover)	24.9	(0%)	55.3	(0%)	−30.4	(0%)
Daily mean traffic (no diurnal)	30.1	(21%)	53.8	(−2%)	−23.9	(−21%)
Clear sky (clear sky)	23.1	(−7%)	70.1	(27%)	−47.0	(55%)
Maximum overlap (max overlap)	21.7	(−13%)	48.7	(−12%)	−27.0	(−11%)

Note. The numbers in parentheses show the percentage differences with respect to the reference case. All cases assume a contrail vertical thickness of approximately 1,500 m. Solar zenith angles and day lengths at the middle of the month are used to represent the month's SW mean RF based on a five-point Gaussian integration. RF = radiative forcing; IWC = ice water content; LW = long wave; SW = short wave.

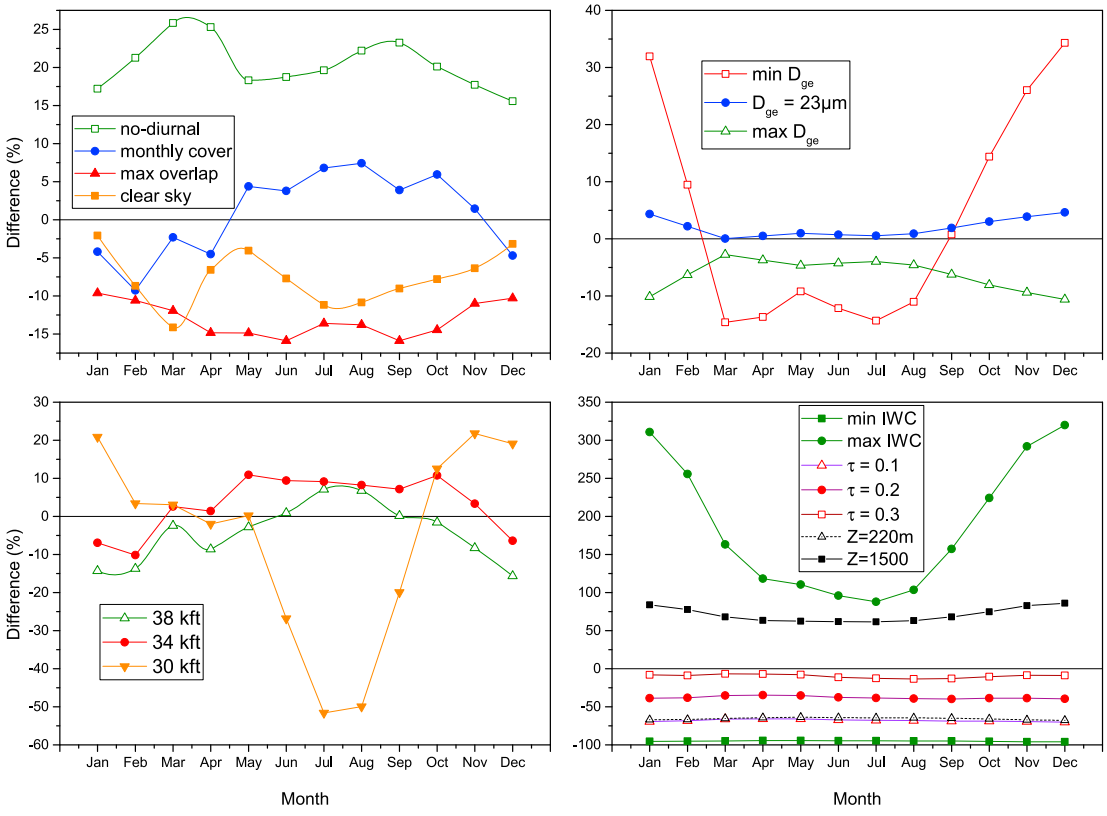

Figure 1. Selected cases of global monthly mean (January–December) contrail net radiative forcing differences (as percentages) with respect to their corresponding reference cases described in Tables 1 and 2 (see Tables 1 and 3 for annual means). IWC = ice water content.

Table 2
Description of the Contrail Radiative Representation Sensitivity Cases

Case	Description
Reference case (Ref)	Same as the reference case in Table 1 (IWC and D_{ge} are functions of temperature with variable altitude) but under clear-sky conditions and assuming a vertical thickness of approximately 750 m
Minimum IWC (min IWC)	Same as Ref but using Schiller et al.'s minimum IWC fit of most frequent (>5%) IWC and their corresponding D_{ge}
Maximum IWC (max IWC)	Same as Ref but using Schiller et al.'s maximum IWC fit of most frequent (>5%) IWC and their corresponding D_{ge}
Minimum D_{ge} (min D_{ge})	Same as Ref but prescribing the same variable D_{ge} as in the min IWC case
Maximum D_{ge} (max D_{ge})	Same as Ref but prescribing the same variable D_{ge} as in the max IWC case
Fixed D_{ge} (D_{ge} = 23 μm)	Same as Ref but assuming D_{ge} = 23 μm
Fixed D_{ge} (D_{ge} − 50%)	Same as Ref but assuming D_{ge} = 12 μm
Fixed D_{ge} (D_{ge} + 50%)	Same as Ref but assuming D_{ge} = 35 μm
Fixed vertical thickness (Z = 220 m)	Same as Ref but with a fixed vertical thickness of 220 m
Fixed vertical thickness (Z = 1,500 m)	Same as Ref but with a vertical thickness of 1,500 m
Fixed altitude (30 kft)	Same as Ref but at a fixed altitude of 30,000 ft (9,100 m)
Fixed altitude (34 kft)	Same as Ref but at a fixed altitude of 34,000 ft (10,400 m)
Fixed altitude (38 kft)	Same as Ref but at a fixed altitude of 38,000 ft (11,600 m)
Fixed optical depth (τ = 0.1)	Same as Ref but with τ = 0.1 and D_{ge} = 23 μm
Fixed optical depth (τ = 0.2)	Same as Ref but with τ = 0.2 and D_{ge} = 23 μm
Fixed optical depth (τ = 0.3)	Same as Ref but with τ = 0.3 and D_{ge} = 23 μm
Fixed Z and τ (38 kft τ = 0.1)	Same as case 38 kft but with τ = 0.1 and D_{ge} = 23 μm
Fixed Z and τ (38 kft τ = 0.2)	Same as case 38 kft but with τ = 0.2 and D_{ge} = 23 μm
Fixed Z and τ (38 kft τ = 0.3)	Same as case 38 kft but with τ = 0.3 and D_{ge} = 23 μm
Fixed τ and altitude (τ = 0.3, 30 kft)	Same as case τ = 0.3 but at a fixed altitude of 30 kft
Fixed τ and altitude (τ = 0.3, 34 kft)	Same as case τ = 0.3 but at a fixed altitude of 34 kft
Fixed τ and altitude (τ = 0.3, 38 kft)	Same as case τ = 0.3 but at a fixed altitude of 38 kft
Fixed Z and D_{ge} (38 kft D_{ge} − 50%)	Same as case 38 kft but with D_{ge} = 12 μm
Fixed Z and D_{ge} (38 kft D_{ge} − 50%)	Same as case 38 kft but with D_{ge} = 35 μm
Fixed ZD_{ge} and τ (38 kft D_{ge} − 50% τ = 0.3)	Same as case 38 kft τ = 0.3 but with D_{ge} = 12 μm
Fixed ZD_{ge} and τ (38 kft D_{ge} − 50% τ = 0.3)	Same as case 38 kft τ = 0.3 but with D_{ge} = 35 μm

Note. IWC = ice water content.

The maximum random overlap case, in which a maximum overlap is assumed between vertically contiguous cloudy layers while a random overlap is assumed otherwise, produced a net RF reduction (−13%) similar to the one reported in Yi et al. (2012) (−13.9%) despite the fact that their simulations assumed a fixed altitude.

3.2. Sensitivity to Microphysical Parameters

The simplified contrail representations were assessed by prescribing fixed values for the contrail layer's altitude, vertical thickness, optical thickness (τ), and D_{ge}, one at a time and in combinations. A new reference case for these simulations, described in Table 2, assumed the complex contrail radiative representation described in the methodology and a likely more realistic contrail vertical thickness of around 750 m. All the simulations in Table 2, with the exception of the ones with a fixed τ or other specified fixed vertical thickness, assumed this value. For reasons explained previously, these simulations were performed under clear-sky conditions, which was expected to have a modest effect on the calculated net RF compared to other simplifications assessed in the present section. The results of these sensitivity cases are presented in Table 3 and in Figure 1 and can be compared to the monthly mean RFs of the new reference case shown in Figure 2, which produced LW, SW,

Table 3
Global Annual Mean Contrail Radiative Forcing Assuming a Contrail Vertical Thickness of Approximately 750 m Under Clear-Sky Conditions

	Radiative forcing (mW m^{-2})					
Case	NET		LW		SW	
Reference case (Ref) (Z = 750 m)	13.5		41.2		−27.7	
Minimum IWC (min IWC)	0.7	(−95%)	3.1	(−92%)	−2.5	(−91%)
Maximum IWC (max IWC)	39.5	(194%)	143.4	(248%)	−103.9	(274%)
Minimum D_{ge} (min D_{ge})	14.0	(5%)	65.9	(60%)	−51.9	(87%)
Maximum D_{ge} (max D_{ge})	12.6	(−6%)	34.2	(−17%)	−21.6	(−22%)
Fixed D_{ge} (D_{ge} = 23 μm)	13.7	(2%)	44.4	(8%)	−30.7	(11%)
Fixed D_{ge} (D_{ge} − 50%)	13.2	(−2%)	71.2	(73%)	−58.0	(109%)
Fixed D_{ge} (D_{ge} + 50%)	12.1	(−9%)	32.1	(−22%)	−20.0	(−28%)
Fixed vertical thickness (Z = 220 m)	4.6	(−66%)	16.1	(−61%)	−11.5	(−59%)
Fixed vertical thickness (Z = 1,500 m)	23.1	(72%)	70.1	(70%)	−47.0	(69%)
Fixed h (30 kft)	13.2	(−1%)	67.7	(64%)	−54.5	(96%)
Fixed h (34 kft)	13.8	(3%)	44.0	(7%)	−30.2	(9%)
Fixed h (38 kft)	12.7	(−6%)	34.9	(−15%)	−22.3	(−20%)
Fixed optical depth (τ = 0.1)	4.3	(−68%)	13.5	(−67%)	−9.2	(−67%)
Fixed optical depth (τ = 0.2)	8.3	(−38%)	26.0	(−37%)	−17.7	(−36%)
Fixed optical depth (τ = 0.3)	12.2	(−9%)	37.5	(−9%)	−25.3	(−9%)
Fixed h and τ (38 kft τ = 0.1)	4.8	(−62%)[a]	13.9	(−60%)[a]	−9.1	(−59%)[a]
Fixed h and τ (38 kft τ = 0.2)	9.3	(−27%)[a]	26.7	(−24%)[a]	−17.4	(−22%)[a]
Fixed h and τ (38 kft τ = 0.3)	13.5	(7%)[a]	38.5	(10%)[a]	−25.0	(12%)[a]
Fixed τ and h (τ = 0.3, 30 kft)	6.6	(−45%)[b]	32.0	(−15%)[b]	−25.4	(0%)[b]
Fixed τ and h (τ = 0.3, 34 kft)	10.9	(−10%)[b]	36.1	(−4%)[b]	−25.2	(−1%)[b]
Fixed τ and h (τ = 0.3, 38 kft)	13.5	(11%)[b]	38.5	(3%)[b]	−25.0	(−1%)[b]
Fixed h and D_{ge} (38 kft D_{ge} − 50%)	14.1	(11%)[a]	61.9	(77%)[a]	−47.8	(115%)[a]
Fixed h and D_{ge} (38 kft D_{ge} + 50%)	11.2	(−12%)[a]	26.9	(−23%)[a]	−15.7	(−29%)[a]
Fixed h D_{ge} and τ (38 kft D_{ge} − 50% τ = 0.3)	7.9	(−41%)[c]	35.2	(−9%)[c]	−27.3	(+9%)[c]
Fixed h D_{ge} and τ (38 kft D_{ge} + 50% τ = 0.3)	16.6	(24%)[c]	39.8	(3%)[c]	−23.2	(−7%)[c]

Note. The numbers in parentheses show the percentage differences with respect to the reference case. τ = 0.3. IWC = ice water content.
[a]Refers to differences with respect to case 38 kft. [b]Refers to differences with respect to case τ = 0.3. [c]Refers to differences with respect to case 38 kft.

and net RF global annual mean values of 41.2, −27.7, and 13.5 mW m^{-2}, respectively, and showed a strong seasonal and regional variability, depicted in the geographical distribution of the monthly mean RFs for May and September in Figure 3. Around these months the magnitudes of the calculated SW, LW, and net RFs reached their maximum and minimum global mean values, respectively (see Figure 2). The regional net RF showed seasonal differences between Europe and the United States, with the United States following the global seasonal trend, with its minimum in September and maximum in May, while Europe showed its peak around January and its minimum around July. Locally, the maximum net RF in May was obtained within the United States, where it exceeded 900 mW m^{-2} compared with 450 mW m^{-2} in September, while the local maximum in Europe reached around 600 mW m^{-2} in May and 350 mW m^{-2} in September. On the annual mean, Europe and the United States showed similar local maxima exceeding 500 mW m^{-2}. Similar annual maxima were also obtained by Minnis et al. (1999), for a similar contrail cover (0.09%), by assuming a fixed optical depth of 0.3, despite their global annual RF (20 mW m^{-2}) being larger than the one found here.

The sensitivity to the contrail IWC variability in the complex representation was initially assessed by prescribing the minimum and maximum IWC fits from Schiller et al. (2008) for the most frequent (>5%) IWC measured values in their database, while allowing D_{ge} to vary with the prescribed IWC. Prescribing the minimum IWC fit

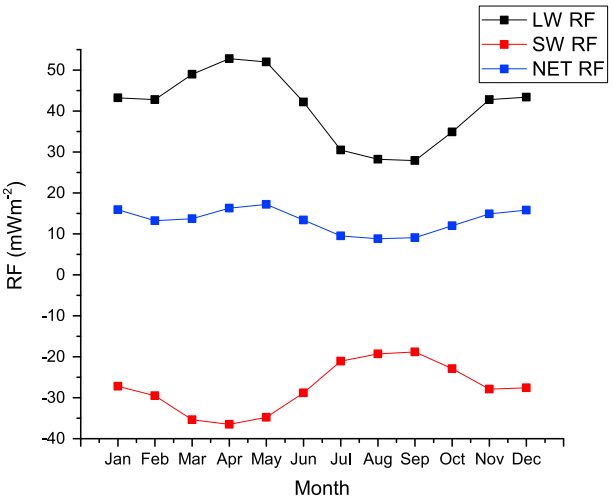

Figure 2. Global monthly mean (January–December) contrail short-wave (SW), long-wave (LW), and NET radiative forcings (RFs) for the reference case described in Table 2.

resulted in a net RF reduction of 95%, with respect to the reference case, while the maximum IWC produced a 194% increase, compared to differences of only +5% and −6% when prescribing mean IWC values and the corresponding minimum and maximum D_{ge}. These differences, and their monthly means, shown in Figure 1, confirmed the preponderant role of the contrails' IWC in the complex representation, but given that extreme values from local measurements are not likely to be representative on a global scale, more realistic cases of IWC and D_{ge} variability ranges were also simulated.

The fixed particle size simulations incorporated a commonly assumed contrail PSD, given in Strauss et al. (1997), for which the calculated D_{ge} = 23 μm was prescribed, while the IWC was allowed to vary. This case showed a net RF difference of only +2% with the reference case, while increasing/decreasing this fixed D_{ge} value by 50% (cases D_{ge} +50% and D_{ge} − 50%) produced annual mean forcing differences of −2% and +9%, respectively. This uncertainty is similar to the one obtained when the minimum and maximum variable D_{ge} fits were prescribed. The monthly mean net RF differences in Figure 1 for the minimum D_{ge} case show changes of sign that can be explained by the fact that bimodal PSDs tend to show small or even negative net RFs for both very small and very large effective particle sizes

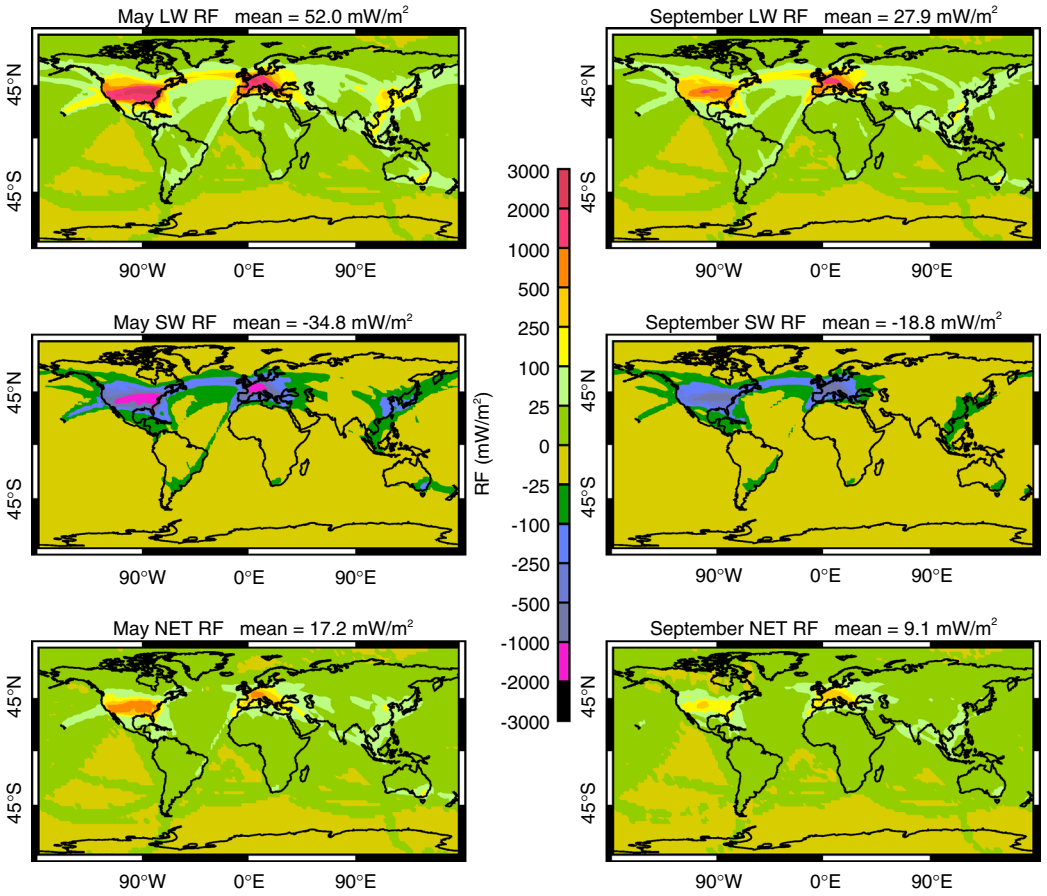

Figure 3. May and September monthly mean short-wave (SW), long-wave (LW), and net (NET) contrail radiative forcings (mW m^{-2}) for the reference case in Tables 2 and 3, assuming a contrail vertical thickness of approximately 750 m, under clear-sky conditions. Solar zenith angles and day lengths at the middle of the month are used to represent the month's SW mean radiative forcing (RF) based on a five-point Gaussian integration.

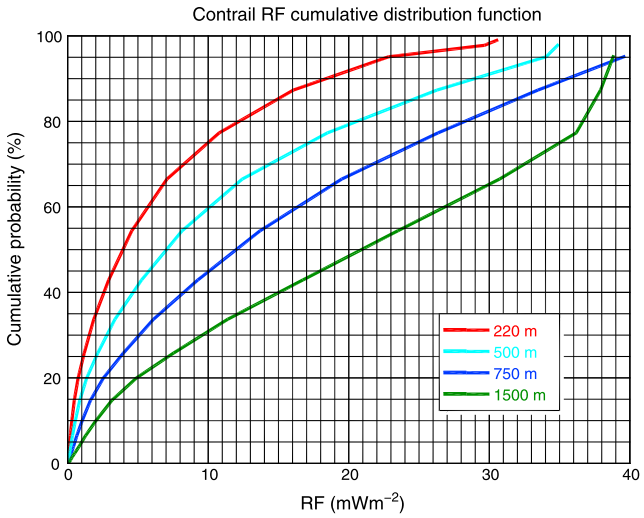

Figure 4. Cumulative probability density functions of clear-sky contrail radiative forcing (RF) (mW m^{-2}) for three assumed contrail vertical thickness values, based on ice water content probability distributions at temperatures between 220 and 224 K.

(see Figure 6 in Zhang et al., 1999) and also by the fact that small effective particle sizes show an already strong SW RF that is enhanced during the longer days during the boreal summer months.

In order to emulate different contrail vertical thickness values, the prescribed IWC was scaled to reduce the ice water path of the original model layer's vertical thickness (~1,500 m). Two assumed values (220 and 1,500 m) produced a RF range [5, 23 mW m^{-2}] with differences between −66% and +72% with respect to the reference case, in which a thickness of 750 m was assumed. The global annual mean optical depth for the relevant contrail layers, at altitudes between approximately 25,000 and 45,000 ft (7,600 m and 13,700 m) in our model, was 0.35 when assuming a vertical thickness of 750 m, scaling linearly with vertical thickness. The relationship between the calculated contrail RF and the contrails' vertical thickness is better depicted in Figure 4 by cumulative distribution functions for four contrail vertical thickness values (220, 500, 750, and 1,500 m). These functions, based on probability distributions of the IWC at a representative contrail temperature range [220 to 224 K], can be used to estimate the likelihood of the calculated contrail RFs for different vertical thickness assumptions in our model. There are currently no climatological data available on contrail vertical thickness. Freudenthaler et al. (1995) reported a range for contrails persistent for up to 60 min, consistent with our two smaller chosen values (220 and 750 m), which produced contrail RFs of 5 and 13 mW m^{-2}, respectively. The RF estimate reported by Lee et al. (2009) for the year 2005 (11.8 mW m^{-2}) falls at the higher end of this range, and in our model setup this RF would imply a contrail thickness of around 700 m. A probably more representative 500 m thickness in our setup resulted in a RF of 9 mW m^{-2}. From Figure 4, assuming a 500 m thickness and a 2/3 likelihood on the IWC's variability implies a contrail RF range between 1 and 23 mW m^{-2}, which provides a more conservative estimate of the RF dependence on IWC variability than the one based on minimum and maximum IWC fits.

In the altitude sensitivity simulations a vertically integrated single layer contrail cover was allocated at fixed altitudes, covering a range of values commonly used in contrail studies. These altitudes were defined by three specified model pressure levels (300, 250, and 200 hPa) with their base at roughly 30,000 ft, 34,000 ft, and 38,000 ft (9,100 m, 10,400 m, and 11,600 m), respectively. This setup allowed the dependence of the contrail radiative properties on altitude to be isolated from those of contrail formation. The global mean net RFs of the fixed altitude cases showed a modest sensitivity, with the monthly differences in Figure 1, reflecting the competition between the enhanced/reduced LW RF at high/low altitudes and the enhanced/reduced SW RF contribution during the boreal summer/winter.

The fixed τ sensitivity simulations comprised a range of values commonly assumed in contrail studies [0.1 to 0.3], which produced a contrail RF range [4 to 12 mW m^{-2}] and differences between −68% and −9% with the reference case. The same range of fixed optical depths combined with a fixed altitude (38,000 ft) produced a similar net RF range [5 to 13 mW m^{-2}] and uncertainty, with differences between −62% and +7% with respect to the case that assumed the same fixed altitude and a complex representation (case 38 kft).

Combining the prescribed altitude range with a fixed optical depth of 0.3 resulted in differences between −45% and +11% with respect to case τ = 0.3, in which altitude was allowed to vary. In contrast, relatively modest differences, between −6% and +3%, were obtained in the complex representation by, instead of prescribing a fixed optical depth, allowing the IWC and D_{ge} to vary with altitude.

The particle size sensitivity was also assessed at a fixed altitude of 38,000 ft (cases 38 kft D_{ge} +50% and 38 kft D_{ge} − 50% in Tables 2 and 3, not shown in Figure 1) which resulted in differences, with respect to case 38 kft, of −12% and +11%, respectively, but the largest differences from the fixed particle size simulations occurred when the optical depth was also fixed (case 38 kft D_{ge} − 50% τ = 0.3 and case 38 kft D_{ge} +50% τ = 0.3), which produced differences with case 38 kft τ = 0.3 of −41% and +24%, respectively. These results confirmed the large uncertainty reported by Yi et al. (2012), who found differences between −5.4% and 45.9% with a similar setup. In contrast, the three cases in which only the particle size was fixed, despite covering the same D_{ge} range, produced an uncertainty of only around 10% if the IWC's dependence on temperature is accounted for.

4. Discussion and Conclusions

Simplified representations of the radiative properties of persistent linear contrails in large-scale applications can offer important advantages, such as providing more transparent setups for model intercomparison studies (e.g., Myhre et al., 2009), but when estimating their RF and associated uncertainties, it is of paramount importance to understand the effect of these simplifications. With this aim in mind, a complex temperature-dependent parameterization of the radiative properties of persistent contrails was implemented and compared to simplified setups in which the complex representation was replaced by fixed values for the relevant variables. This representation was applied to a diurnally resolved 3-D linear contrail cover, assuming the same dependence of contrail properties on temperature as for natural cirrus, and in which only the contrails' vertical extent, for which there is currently no climatological data available, was assumed constant.

The complex representation setup showed a contrail net RF enhancement by natural clouds over regions with low albedo, but on the global mean a 7% net RF reduction was obtained. The assumed cloud overlap resulted in an uncertainty of 13%, similar to a previous study by Yi et al. (2012). The inclusion of the monthly traffic variability produced negligible differences. In contrast, a 21% reduction resulted from neglecting its diurnal variability, which increased the nighttime net RF contribution from 84% to 86%, and confirmed the disproportional contribution of nighttime traffic reported by Chen and Gettelman (2013) (92%) despite only representing 38% of the total distance in our study.

Prescribing fixed τ values resulted in differences covering a factor of 3, and similar differences were obtained when combining the same range of optical depths with a fixed altitude. The prescribed range of fixed altitudes produced differences of only around 10% in the complex representation, compared to a factor of 2 when prescribing a fixed $\tau = 0.3$. Similarly, fixing the ice particle diameter between 12 and 35 μm resulted in differences of only around 10% in the complex representation, compared to differences of more than 20% when also fixing altitude. Much larger differences, covering a factor of 2, were obtained when also fixing $\tau = 0.3$. Previous off-line contrail RF estimates based on these fixed variable assumptions may be similarly affected by these simplifications, contributing or adding to the uncertainty reported by Myhre et al. (2009) in their model intercomparison.

Assuming minimum/maximum values for the contrails' D_{ge} and IWC in the complex representation confirmed the IWC's preponderant role in determining the range of contrail RFs. A 2/3 likelihood on the IWC's variability resulted in a contrail RF range between 1 and 23 mW m^{-2} when prescribing a contrail vertical thickness of 500 m. This range provided an estimate of the contrail RF uncertainty associated to the IWC's variability in our model setup, as well as context from the perspective of the complex representation to the uncertainties reported by Lee et al. (2009) [5.4 to 25.6 mW m^{-2}] and by Boucher et al. (2013) [5 to 30 mW m^{-2}]. The RF range [4 to 12 mW m^{-2}] that resulted from prescribing commonly assumed fixed optical depths (0.1 to 0.3) fell in the lower end of these published uncertainties. From these results it was concluded that the dependence of the IWC on temperature provided a much improved representation of the radiative properties, reducing the dependence of their estimated RF on the uncertainties linked to contrail altitude and ice particle size.

Acknowledgments
This work was supported by the United Kingdom Department for Transport and by the European Union FP7 project REACT4C (React for climate: http://www.react4c.eu/). The traffic data used in this study are available through the REACT4C Project to noncommercial users after signing a data agreement. The permanent URL is http://www.react4c.eu/data/, last accessed on 15 October 2017. The ice water content and particle size distribution parameterizations were derived from the formulae and coefficients (Table 2) in Schiller et al. (2008) and (Tables 1 and 2) in McFarquhar and Heymsfield (1997). Any opinions, findings, and conclusions or recommendations expressed in this paper are those of the authors and do not necessarily reflect the views of the sponsors.

References

Baran, A. J., Havemann, S., & Mackowski, D. (2001). A database of hexagonal column optical properties for wavelengths ranging between 0.2 microns to 30 microns produced for ANNEX 7. Contract No. 4b/3/02, DEFRA, UK, 2001.

Boucher, O., Randall, D., Artaxo, P., Bretherton, C., Feingold, G., Forster, P., et al. (2013). Clouds and aerosols supplementary material. In T. F. Stocker et al. (Eds.), *The Physical Science Basis. Contribution of Working Group I to the Fifth Assessment Report of the Intergovernmental Panel on Climate Change*. Cambridge, UK: Cambridge University Press. Retrieved from https://www.climatechange2013.org and https://www.ipcc.ch

Chauvigné, A., Jourdan, O., Schwarzenboeck, A., Gourbeyre, C., Voigt, C., Schlager, H., et al. (2017). Statistical Analysis of Contrail to Cirrus Evolution during the Contrail and Cirrus Experiments (CONCERT). *Atmospheric Chemistry and Physics Discussion*, 1–27.

Chen, C.-C., & Gettelman, A. (2013). Simulated radiative forcing from contrails and contrail cirrus. *Atmospheric Chemistry and Physics*, *13*, 12,525–12,536.

De León, R. R., & Haigh, J. D. (2007). Infrared properties of cirrus clouds in climate models. *Quarterly Journal of the Royal Meteorological Society*, *133*, 273–282.

De León, R. R., Krämer, M., Lee, D. S., & Thelen, J. C. (2012). The sensitivity of radiative properties of persistent contrails to the ice water path. *Atmospheric Chemistry and Physics*, *12*, 7893–7901.

Edwards, J. M., & Slingo, A. (1996). Studies with a flexible new radiation code. I: Choosing a configuration for a large-scale model. *Quarterly Journal of the Royal Meteorological Society*, *122*, 689–719.

Freudenthaler, V., Homburg, F., & Jäger, H. (1995). Conrail observations by ground-based scanning lidar: Cross-sectional growth. *Geophysical Research Letters*, *9*, 3501–3504.

Frömming, C., Ponater, M., Burkhardt, U., Stenke, A., Pechtl, S., & Sausen, R. (2011). Sensitivity of contrail coverage and contrail radiative forcing to selected key parameters. *Atmospheric Environment*, *45*(7), 1483–1490.

Fu, Q. (1996). An accurate parameterization of the solar radiative properties of cirrus clouds for climate models. *Journal of Climate*, *9*, 2058–2082.

Krämer, M., Rolf, C., Luebke, A., Afchine, A., Spelten, N., Costa, A., et al. (2016). A microphysics guide to cirrus clouds. Part 1: Cirrus types. *Atmospheric Chemistry and Physics*, *16*, 3463–3483.

Krämer, M., Schiller, C., Afchine, A., Bauer, R., Gensch, I., Mangold, A., et al. (2009). Ice supersaturations and cirrus cloud crystal numbers. *Atmospheric Chemistry and Physics*, *9*(11), 3505–3522.

Lee, D. S., Fahey, D. W., Forster, P. M., Newton, P. J., Wit, R. C., Lim, L. L., & Sausen, R. (2009). Aviation and global climate change in the 21st century. *Atmospheric Environment*, *43*(22-23), 3520–3537.

Lim, L. L., Rodríguez De León, R., & Lee, D. S. (2015). Uncertainties with respect to contrail coverage modelling in REACT4C. In R. Sausen, A. Blum, D. S. Lee, & C. Brüning (Eds.), *Proceedings of an International Conference on Transport, Atmosphere and Climate (TAC)* (pp. 279–283). Deutsches Zentrum für Luft- und Raumfahrt (DLR). Oberpfaffenhofen, Deutschland: Institut für Physik der Atmosphäre.

Lim, L. L., Lee, D. S., Ismail, R., Grainger, R. G., Gierens, K., & Ponater, M. (2006). Comparison of cirrus cloud coverage calculated from reanalysis meteorological data with satellite data. In R. Sausen, S. Unterstrasser, & A. Blum (Eds.), *Proceedings of the 4th International Conference on Transport, Atmosphere and Climate (TAC-4)*, Deutsches Zentrum für Luft- und Raumfahrt (DLR). Oberpfaffenhofen, Deutschland: Institut für Physik der Atmosphäre.

Markowicz, K. M., & Witek, M. L. (2011). Simulations of contrail optical properties and radiative forcing for various crystal shapes. *Journal of Applied Meteorology and Climatology*, *50*, 1740–1755.

McFarquhar, G. M., & Heymsfield, A. J. (1997). Parameterization of tropical cirrus ice crystal size distributions and implications for radiative transfer: Results from CEPEX. *Journal of the Atmospheric Sciences*, *54*, 2187–2200.

Minnis, P., Schumann, U., Doelling, D. R., Gierens, K., & Fahey, D. (1999). Global distribution of contrail radiative forcing. *Geophysical Research Letters*, *26*, 1853–1856.

Myhre, G., & Stordal, F. (2001). On the tradeoff of the solar and thermal infrared radiative impact of contrails. *Geophysical Research Letters*, *28*(16), 3119–3122.

Myhre, G., Kvalevåg, M., Shine, K. P., Rädel, G., Cook, J., Clark, H., et al. (2009). Quantifying the uncertainty associated with the radiative forcing of stratospheric water vapour and contrails. *Meteorologische Zeitschrift*, *18*(6), 585–596.

Ponater, M., Brinkop, S., Sausen, R., & Schumann, U. (1996). Simulating the global atmospheric response to aircraft water vapour emissions and contrails—A first approach using a GCM. *Annales Geophysicae*, *107*(D13), 941–960.

Rädel, G., & Shine, K. P. (2008). Radiative forcing by persistent contrails and its dependence on cruise altitudes. *Journal of Geophysical Research*, *113*, D07105. https://doi.org/10.1029/2007JD009117

Rap, A., Forster, P. M., Jones, A., Boucher, O., Haywood, J. M., Bellouin, N., & De Leon, R. R. (2010). Parameterization of contrails in the UK Met Office Climate Model. *Journal of Geophysical Research*, *115*, D10205. https://doi.org/10.1029/2009JD012443

Sausen, R., Gierens, K., Ponater, M., & Schumann, U. (1998). A diagnostic study of the global distribution of contrails Part I: Present day climate. *Theoretical and Applied Climatology*, *61*(3–4), 121–141.

Schäuble, D., Voigt, C., Kärcher, B., Stock, P., Schlager, H., Krämer, M., et al. (2009). Airborne measurements of the nitric acid partitioning in persistent contrails. *Atmospheric Chemistry and Physics*, *9*, 8189–8197.

Schiller, C., Kramer, M., Afchine, A., & Spelten, N. (2008). Ice water content of Arctic, midlatitude, and tropical cirrus. *Journal of Geophysical Research*, *113*, D24208. https://doi.org/10.1029/2008JD010342

Simmons, A., & Gibson, J. (2000). The ERA-40 Project Plan, ERA-40 Project Report Series 1.

Søvde, O. A., Matthes, S., Skowron, A., Iachetti, D., Lim, L., Owen, B., et al. (2014). Aircraft emission mitigation by changing route altitude: A multi-model estimate of aircraft NO_x emission impact on O_3 photochemistry. *Atmospheric Environment*, *95*, 468–479.

Strauss, B., Meerkoetter, R., Wissinger, B., Wendling, P., & Hess, M. (1997). On the regional climatic impact of contrails: Microphysical and radiative properties of contrails and natural cirrus clouds. *Annales Geophysicae*, *15*(11), 1457–1467.

Stuber, Nicola, & Forster, P. (2008). The impact of diurnal variations of air traffic on contrail radiative forcing. *Atmospheric Chemistry and Physics*, *7*, 3153–3162.

Waliser, D. E., Li, J. L. F., Woods, C. P., Austin, R. T., Bacmeister, J., Chern, J., et al. (2009). Cloud ice: A climate model challenge with signs and expectations of progress. *Journal of Geophysical Research*, *114*, D00A21. https://doi.org/10.1029/2008JD010015

Yang, P., Liou, K. N., Wyser, K., & Mitchell, D. (2000). Parameterization of the scattering and absorption properties of individual ice crystals. *Journal of Geophysical Research*, *105*, 4699–4718.

Yi, B., Yang, P., Liou, K. N., Minnis, P., & Penner, J. E. (2012). Simulation of the global contrail radiative forcing: A sensitivity analysis. *Geophysical Research Letters*, *39*, L00F03. https://doi.org/10.1029/2012GL054042

Zhang, Y., Macke, A., & Albers, F. (1999). Effect of crystal size spectrum and crystal shape on stratiform cirrus radiative forcing. *Atmospheric Research*, *52*(1), 59–75.